

Quasi-monochromatic field-emission x-ray source

Babacar Diop and Vu Thien Binh

Citation: *Rev. Sci. Instrum.* **83**, 094704 (2012); doi: 10.1063/1.4752406

View online: <http://dx.doi.org/10.1063/1.4752406>

View Table of Contents: <http://rsi.aip.org/resource/1/RSINAK/v83/i9>

Published by the [American Institute of Physics](#).

Related Articles

Synchrotron-based coherent scatter x-ray projection imaging using an array of monoenergetic pencil beams
Rev. Sci. Instrum. **83**, 095114 (2012)

The x-ray source application test cassette for radiation exposures at the OMEGA laser
Rev. Sci. Instrum. **83**, 10E136 (2012)

Glancing angle Talbot-Lau grating interferometers for phase contrast imaging at high x-ray energy
Appl. Phys. Lett. **101**, 091108 (2012)

Note: Measurement of extreme-short current pulse duration of runaway electron beam in atmospheric pressure air
Rev. Sci. Instrum. **83**, 086106 (2012)

A silicon 111 phase retarder for producing circularly polarized x-rays in the 2.1-3keV energy range
Appl. Phys. Lett. **101**, 064107 (2012)

Additional information on *Rev. Sci. Instrum.*

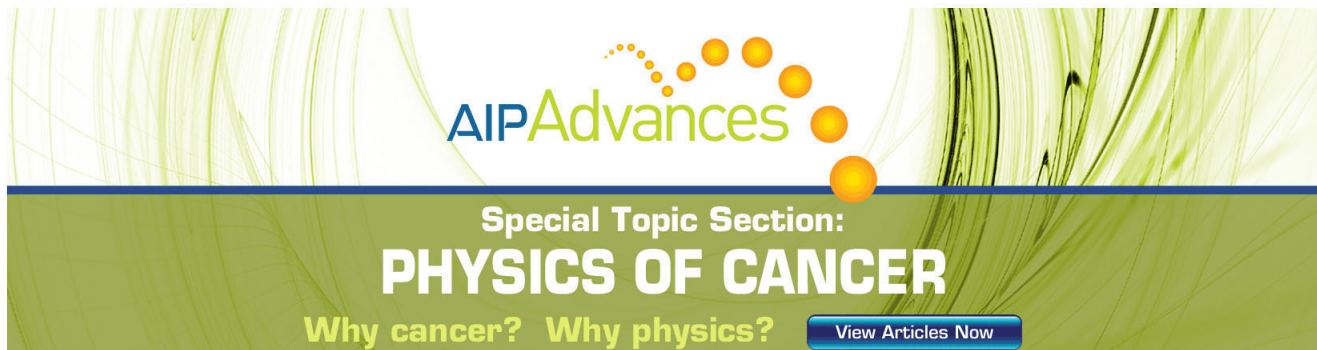
Journal Homepage: <http://rsi.aip.org>

Journal Information: http://rsi.aip.org/about/about_the_journal

Top downloads: http://rsi.aip.org/features/most_downloaded

Information for Authors: <http://rsi.aip.org/authors>

ADVERTISEMENT



AIP Advances

Special Topic Section:
PHYSICS OF CANCER

Why cancer? Why physics? [View Articles Now](#)

Quasi-monochromatic field-emission x-ray source

Babacar Diop^{a)} and Vu Thien Binh^{b)}

LPMCN, University of Lyon 1, Villeurbanne 69622, France

(Received 8 April 2012; accepted 29 August 2012; published online 25 September 2012)

By favoring the L-peak emission over the bremsstrahlung part, direct quasi-monochromatic soft x-ray emission has been obtained with a field emission (FE) x-ray source. The electron impact x-ray setup uses an arrayed cathode of carbon nanopearl FE tips as a stable cold electron source within a vacuum of 10^{-6} – 10^{-7} Torr. The high brightness of the FE e-beam coupled with the array structure of the cold cathode allows a smoother control of the x-ray emission intensity. The wavelength of the x-ray source can be modified by the choice of target materials. Using Mo as the target material, the x-ray emission shows a peak centered at 2.45 keV with a monochromaticity between 75% and 55% and a FWHM in the range of 450 eV. © 2012 American Institute of Physics. [<http://dx.doi.org/10.1063/1.4752406>]

I. INTRODUCTION

While most technologies required for the application of x-rays in various areas – such as surface analysis, (nano)lithography, microradiology, micro-computer tomography, or localized radiotherapy – are now well known and available, two major challenges remain with regards to the x-ray source. The first one: the inadequacy of one of its most critical components, the electron source. In fact, the thermionic emission is not efficient enough for low-powered miniaturized x-ray tubes mainly because of the dissipation of heat radiated from the hot filament resulting from a very low yield for thermal electron emission. Thus, the alternate means to generate electrons by field emission (FE) presents many advantages. However, the potential benefits of FE for x-ray sources can only be achieved with field emitters that would be mechanically, chemically, and electrically robust enough within the specific working conditions of x-ray tubes and in particular in poor vacuum, in the range of 10^{-6} Torr, which induces strong cation sputtering during operation. This is the reason why conventional FE metallic tips have not found practical application in x-ray tubes because they were soon damaged by cation sputtering or thermal runaway due to adsorption.¹ It is only recently that electron impact (e-impact) x-ray sources experienced new technological development with regards to the use of carbon nanotubes (CNTs) for FE cathodes,² in particular in the field of effective miniaturization³ and high resolution imaging.⁴

The second challenge to overcome is the achievement of a monochromatic x-ray source, which has not been achieved yet in spite of numerous attempts. Amongst them are the filtration techniques which mainly include the differential filtering of the bremsstrahlung emission,^{5,6} the x-ray differential reflection from monochromating crystals or multilayers, the production of fluorescence x-rays from secondary targets, and the directional enhancement of characteristic peaks relative to bremsstrahlung by thin foils.⁷ Nevertheless, not only the loss

of x-ray signal intensity is important due to the filtering processes used, but the resulting x-ray spectrum still includes a non-negligible continuous bremsstrahlung part vs. characteristic peaks, i.e., the x-ray still remains mostly polychromatic.

In this paper, we present an approach to reach directly, i.e., without the filtering step, a quasi-monochromatic soft x-ray source with a high monochromaticity value, by restraining the energy spectrum to the L-shell characteristic peaks of the anode element. This approach has been enabled by the high brightness of the e-beam of carbon nanopearl (CNP) FE cathode⁸ and its stability within working vacuum in the range of 10^{-6} Torr.

II. CONCEPT FOR A DIRECT MONOCHROMATIC SOFT X-RAY SOURCE

In the e-impact process for the production of x-rays the photon spectrum includes (1) the bremsstrahlung radiation, which is a polychromatic part due to the deflection of incident electrons by atomic nuclei, and (2) the characteristic lines (peaks) resulting from L- or K-shell ionization when a bombarding electron interacts with an atomic electron and ejecting it from its electronic shell (Fig. 1).

The probability of x-ray production by bremsstrahlung interaction is energy dependant and the theoretical model for thick target⁹ – with simplifying assumptions and without target attenuation – provides a simple relation for its intensity between E_X and $E_X + dE_X$,

$$E_X N(E_X) dE_X = \text{const} \times Z \times (E_e - E_X) dE_X, \quad (1)$$

where E_X is the energy of the x-ray photon produced, $N(E_X)dE_X$ is the number of x-ray photons having an energy between E_X and $E_X + dE_X$ per incident electron, Z is the target atomic number, and E_e is the electron's kinetic energy. Taking into account the target attenuation due to a filtration during the photon escape through the target surface, one transforms the linear decrease of Eq. (1) into a more complicated relation,¹⁰ with a stronger removal of low-energy photon, leading to the well known bremsstrahlung curve with a maximum.

The production of characteristic x-rays lines/peaks from a thick target comes from direct and indirect processes as

^{a)}Present address: Nanomed, Inc., and Concordia University, Montréal, Québec, Canada.

^{b)}Author to whom correspondence should be addressed. Electronic mail: binh.vu-thien@univ-lyon1.fr.

Lines	Cu (keV)	Mo (keV)	
$L\alpha_1$	0.929	2.293	
$L\alpha_2$	0.929	2.290	
$L\beta_1$	0.950	2.395	
$L\beta_2$	/	2.518	
$L\gamma_1$	/	2.623	
$K\alpha_1$	8.047	17.479	
$K\alpha_2$	8.027	17.374	
$K\beta_1$	8.905	19.608	

FIG. 1. X-ray emission energy of the characteristic L- and K-shell lines for Cu and Mo (left side) and the transitions that give rise to the emission lines (right side) (from Ref. 26).

described below

$$I_{K,L} = I_{K,L}(\text{direct}) + I_{K,L}(\text{indirect}), \quad (2)$$

where $I_{K,L}(\text{direct})$ is the contribution from direct Coulomb interaction ionization and $I_{K,L}(\text{indirect})$ from the photoelectric ionization induced by the bremsstrahlung. A combined theoretical and experimental study of L-shell peaks by electron impacts from threshold energy to 30 keV¹¹ gives an empirical formula detailed thereafter

$$I_L = 1.3 \times 10^{-7} \times Z^{1.3} (U_L - 1)^{1.46} \times 0.938^{\ln(U_L - 1)^2}, \quad (3)$$

which can be approximated near the threshold energy by the relation

$$I_L \propto (U_L - 1)^{1.67}, \quad (4)$$

where $U_L > 1$ is the ratio of E_e to the L-shell ionization energy. For a short penetration distance, the characteristic x-ray production increases with depth to a maximum, attributed to the escape of backscattered electrons, followed by a decrease as the electrons loose energy when they penetrate deeper into the target.¹²

Finally, one shall consider the definition of the monochromaticity M of an x-ray peak signal as being the following ratio:⁷

$$M = \frac{\int_{pk_{\min}}^{pk_{\max}} S(E_X) dE_X}{\int_0^{E_{\max}} S(E_X) dE_X}, \quad (5)$$

where $S(E_X)$ is the source spectrum and the integral in the numerator is limited to the interval of the characteristic peak- i [pk_{\min} - pk_{\max}] _{i} , whereas the integral in the denominator covers the whole energy range of the spectrum.

Currently, in order to obtain monochromatic x-rays from e-impact process one can use a filtering technique which implies a post differential attenuation of the x-ray spectra through a filter. In Fig. 2, for example, the pre- and post-filtered spectra produced at 26 keV e-impact energy on Mo anode target illustrated the modification of the x-ray spectrum after a filtration with a Mo 30- μm foil thickness.¹³ It shows a

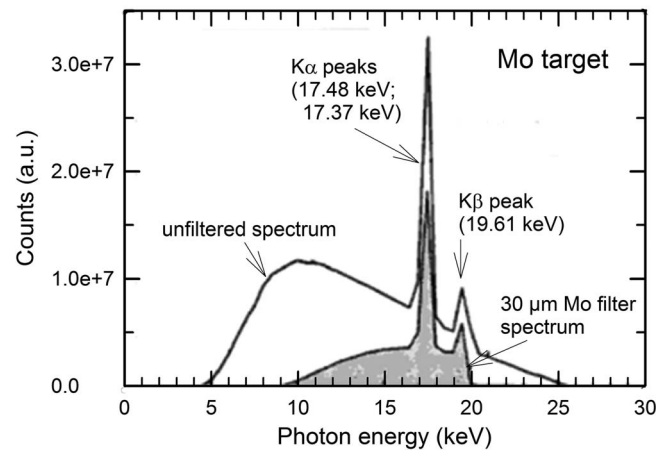


FIG. 2. Mo-anode x-ray spectra produced by an electron energy impact of 26 keV. With and without 30- μm Mo K-edge filtering.¹³

drastic attenuation of x-ray energies above the 20-keV K-edge of Mo, concomitant to a significant reduction of intensity at lower energies. Recently, in order to enhance the characteristic lines of e-impact x-ray source, several authors^{7,14} suggested to use the property of polar dependence of the atomic bremsstrahlung cross-section by observing x-rays from thin foil targets with thickness in the μm range and in a direction anti-parallel to that of the incident beam. However, the substrate where the thin foil should be deposited produced a non-negligible contribution to bremsstrahlung that limits the monochromaticity of the resulting photon spectrum.

In the approach proposed in this article, the monochromaticity of the x-ray signal is obtained by limiting the values of E_e to only obtain the first characteristic peak of photon. This can be reached by restraining the x-ray spectra to the L-shell characteristic peak, which are in general a cluster of the $L_{\alpha,\beta,\gamma}$ emission lines, as illustrated in Fig. 1 for Cu and Mo, for instance. The values of E_e result from a trade-off between the lowest values for Eq. (1) and the highest values for Eqs. (3) and (4).

Concomitantly, the beam quality is evaluated in terms of the FWHM of the energy peak. As the L-shell lines get closer to each other, experimentally, they will merge into a single peak, named L-peak, with a FWHM which turns out to be as important as the number and energy interval between the farthest merging. As an example, for Cu one can assume that the resulting L-peak will be located at ~ 0.94 keV with a FWHM in the range of 20 eV. In the case of Mo, with five L-shell lines between 2.29 and 2.62 keV one can assume that the L-peak will be centered at ~ 2.45 keV with a FWHM in the range of 350 eV which is the interval of energy occupied by those $L_{\alpha,\beta,\gamma}$ lines.

III. EXPERIMENTAL SETUP

A. The field emission x-ray setup

Figure 3 is the schematic representation of our experimental FE x-ray setup. The cubic vacuum chamber ($12 \times 12 \times 12$ cm³) has previously been emptied by a 70-l turbomolecular pump to a working vacuum of 10^{-6} - 10^{-7} Torr. This vacuum can be maintained by an 8-l ion pump,

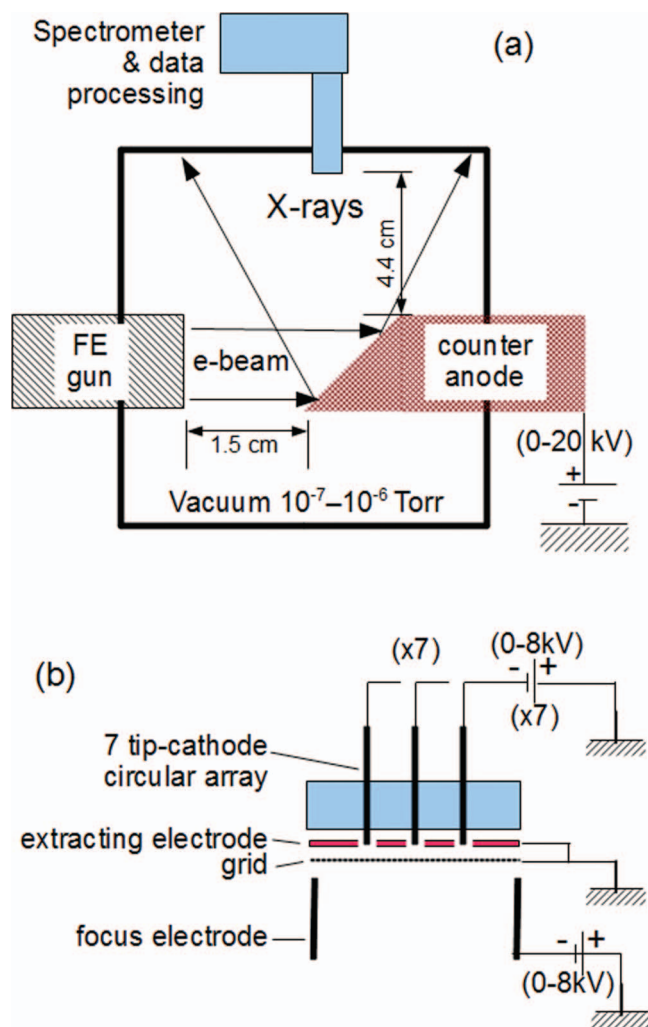


FIG. 3. Experimental arrangement of the FE x-ray setup. (a) Target chamber. (b) Details of the FE gun.

allowing the turbo-pump to shutdown when the working pressure is reached.

The base of the counter-anode is a bulk rod of Cu (2.54 cm diameter) and the irradiated surface was 45° vs. the rod axis. In order to allow a rapid change in the target material, a 500- μm -thick plate composed of various other materials can be fixed on the copper rod in order to define the actual counter-anode element should it be different in composition from Cu. The counter-anode is then connected to a positive 0–20 kV high-voltage supply.

The x-ray energy distribution is obtained via a commercial Amptek[®] CdTe detector.¹⁵ The main drawback of this detector is the very low sensitivity of CdTe material for photon energy of less than ~ 1.2 keV, associated with an intrinsically strong noise peak within the same energy region due to the electronics. Therefore, unambiguous reproducible spectra and characteristic peaks can be obtained and analyzed specifically for energy range greater than ~ 2 keV.

B. The field emission gun

FE consists in the extraction of electrons from a conducting solid by a high electric field in the order of 10^7 V/cm and,

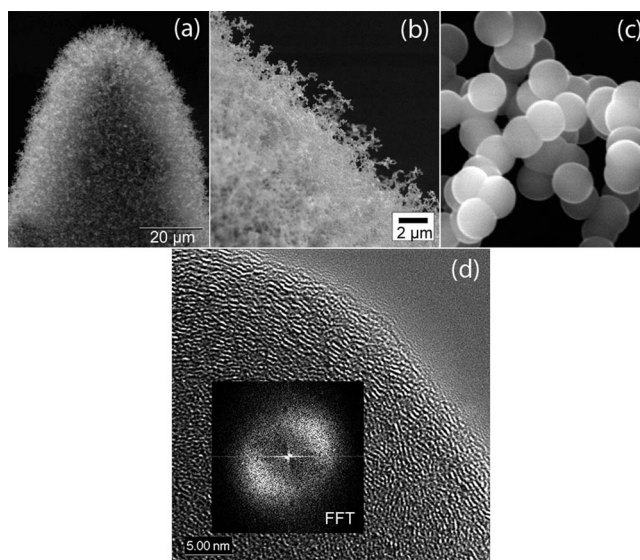


FIG. 4. Carbon nanopearl tip. (a) The carbon nanopearl (CNP) tip is obtained by covering a metallic tip with a layer of carbon nanopearls. (b) Carbon nanopearl emitter surface. (c) A field emission gun-SEM close view of carbon nanopearls. The carbon nanosphere diameter is ~ 100 nm. (d) HRTEM image of the surface of a nanopearl. The orientation of the fringes and the FFT near the surface (inset) indicated a concentric disposition of wavy nanoflakes.

unlike thermionic emission, there is no heat required to obtain electrons to tunnel through the surface potential barrier. The main specificities of the FE cathodes are the following:

- The brightness of FE cathodes is amongst the highest for all electron sources; the cold cathodes usually deliver current densities in the range of 10^5 – 10^9 A/cm², with a theoretical limit of 10^{12} A/cm², in comparison to about 100 A/cm² for thermionic emission.
- Field emitters can be directly switched on and off during the tube operation at high frequencies.
- The cold nature of the emission prevents thermal outgassing and drifts from the cathode, it therefore allows for stable electron focusing system as well as extreme miniaturization to sub-mm range.

Recently, it has been demonstrated that operating a CNT emitter under poor vacuum conditions does not destroy the emitters but only shortens its lifetime.^{16–19} Thereafter, the robustness and long life expectancy of nanocarbon based emitters has been fully exploited with CNP emitters^{8,20,21} (Fig. 4). These CNP tips have already been used successfully as cold electron sources, as an alternative to thermionic cathodes, in conventional time of flight spectrometer and x-ray devices.^{22,23}

When compared to the tubular geometry of CNTs, the nanopearls have the substantial advantage of statistically presenting a high density of apex areas with a small radius of curvature (~ 50 nm) when deposited on a planar surface (Figs. 4(a)–4(c)). Moreover, these nanospheres are composed of graphitic flakes (Fig. 4(d)) that are unclosed at the surface and therefore believed to exhibit many dangling bonds with the potential to enhance the field emission current^{24,25} and the current stability. Figure 5 illustrates the field emission behavior of the CNP cathode and the stability of the field

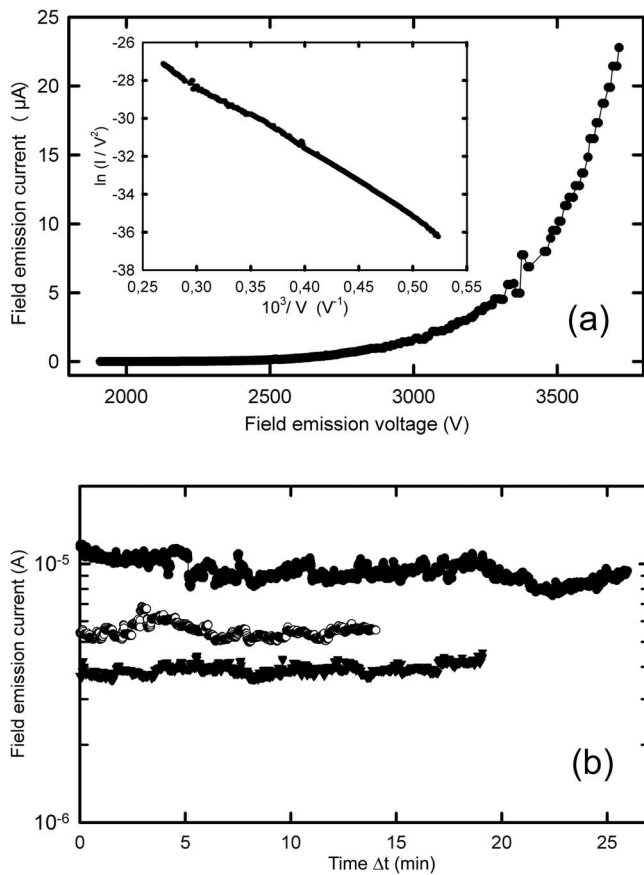


FIG. 5. FE characteristics of CNP-FE cathode within 10^{-6} – 10^{-7} Torr. (a) I - V characteristics; in the inset, the linear dependence of $\ln(I/V^2)$ vs I/V indicates a Fowler-Nordheim behavior for the FE. (b) Stability of the FE currents for intervals of time of 15–25 min; samples of stable FE currents measured for total durations more than 200 h.

emission currents. These two properties make the CNPs an excellent prospect to be a cathode material. Embedding the CNPs within an insulating matrix extends their FE lifetimes. As an example, CNP cathode lifetime is in excess of 200 h in a TOF-mass-spectrometer (TOF-MS) for detection of organic polymer gases up at 5×10^{-5} Torr, without developing filamentous adsorption compounds that are the main cause for a rapid CNT-FE cathode breakdown in this environment.²³ In the present study, the insulating matrix we used is SiO_2 obtained by a sol-gel process.

In our current system, the FE gun (Fig. 3(b)) is composed of a 7-CNP-tip cathode arranged in a circular array of 8 mm diameter; each of them being independently powered. The whole array is located in front of a common electrostatic system composed of an extracting electrode, a grid, and a focus electrode. The FE specificities of each CNP tip are mostly similar from one to another; and the FE currents for each tip can reach 70–100 μA for FE applied voltages in the range of 4–7 kV. Meanwhile, our usual working voltage is in the range of 1.5–3.5 kV, and these values are sufficient to extract currents in the range of few tens of μA from each individual FE tip. For a vacuum in the x-ray chamber in the range of 10^{-7} – 10^{-6} Torr and during a typical run of 5 h, the FE currents are stable. The stability of the CNP cathodes is therefore suitable for an x-ray tube; and regarding its lifetime (in our

experiment, for example), our FE gun was still active for a cumulative working time of more than 150 h in the range of few tens μA . However, the lifetime of the cathodes is decreasing for FE currents in the range of few hundred μA . This behavior can be explained relatively to an increase of the vacuum pressure up to 10^{-5} – 10^{-4} Torr due to a greater degassing process under e-impact, therefore generating a stronger cation erosion of the cathodes as indicated in our former experimental results.²⁰ A solution to this strong cation erosion is a modification of the FE gun structure if very high current e-beams are required. Finally, as our FE cathode is structured as an array of independently powered emitters, an easy regulation of the total e-beam intensity to about 500 μA and for a same FE applied voltage can be modified only by activating, at the same voltage, more or less the number of FE tips in the array.

IV. EXPERIMENTAL PROCEDURE AND RESULTS

A. Choice of counter-anode material

Even if Cu is considered to have a very good theoretical monochromaticity, it in fact is not a good material for this study because its resulting L-peak is located at ~ 0.94 keV. Not only it is located in the low yield region of the detector but also it is covered up by the noise-peak intrinsic to the detector electronics. For unambiguous results one needs to have an L-peak located at an energy level greater than 2 keV and far away from the K-shell lines. Mo with five L-shell lines between 2.29 and 2.62 keV will have an L-peak which is assumed to be at 2.45 keV with a FWHM of about 400 eV. The closest K-shell line is at a level of 17.37 keV. Therefore, we have used a Mo counter-anode for the present study.

B. Experimental results

Two main experimental characteristics are to be emphasized. First of all, we have obtained a quasi-monochromatic spectrum with the only presence of a single L-peak having a high value of M . Second, we shall point out the dependence of the L-peak intensity with the e-impact FE current.

1. Field emission x-ray spectra

In Fig. 6 we have plotted the x-ray spectra for different e-impact energies from 5 to 14 keV. Figure 6(a) indicates a progression of the L-peak intensity as the e-impact energy increases and moves away from the L-shell line threshold (Fig. 7), in agreement with Eqs. (3) and (4). However, as the e-impact energy increases, the bremsstrahlung part also amplified, in agreement with Eq. (1). This evolution is well illustrated in Fig. 6(b), for which the spectra are plotted with normalized counts, clearly showing the development of the bremsstrahlung part. What shall be pointed out is the conservation of the L-peak characteristics, (i.e., centroid at 2.45 keV and FWHM of 450 eV) vs. the e-impact energy. The decrease of the monochromaticity (Fig. 7) simply results from the relative takeover of the bremsstrahlung part in concomitance with the L-peak growth.

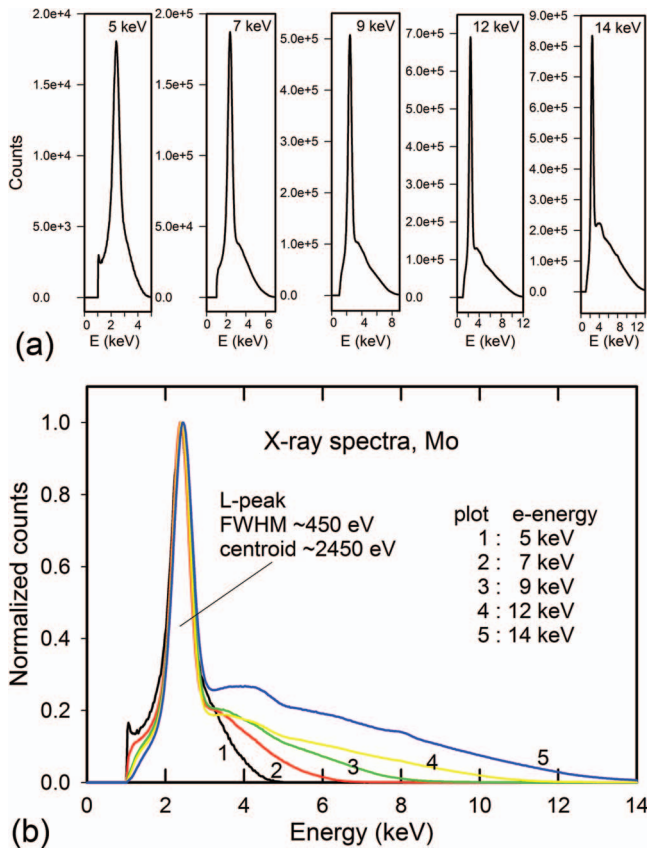


FIG. 6. X-ray spectra for Mo counter-anode and for e-impact energies between 5 and 14 keV for (a) absolute counts and (b) normalized counts.

There is a remark regarding the position of the centroid and the FWHM value of the L-peak: the variations of both values are less than 1% within the same run, i.e., with same settings of the FE gun and spectrometer. These variations increase to 5% between different runs. We assumed that they are due to some deviations in the characteristics of the different settings and, in particular, of the e-beam geometry delivered by the FE gun.

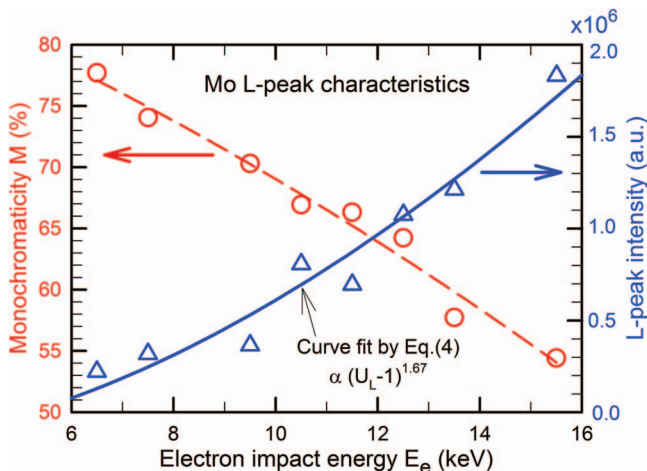


FIG. 7. Mo L-peak monochromaticity and intensity in function of E_e , for the same FE current of $5.5 \mu\text{A}$. The solid (blue) line for the L-peak intensity is a curve fitting with a function proportional to $((E_e/2.52 \text{ keV}) - 1)^{1.67}$.

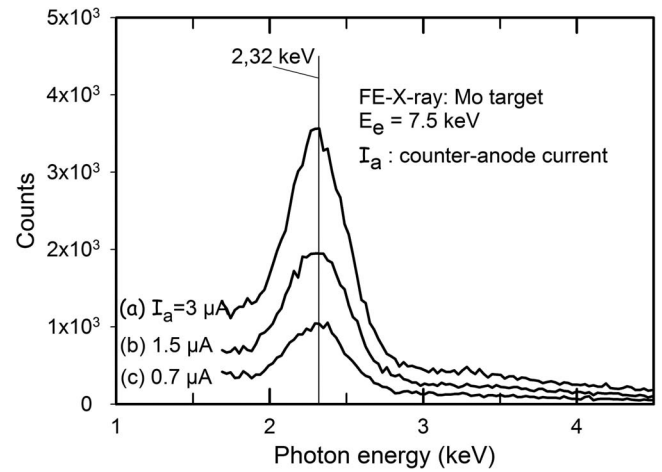


FIG. 8. Evolution of the Mo L-peak for E_e constant vs. 3 different e-beam currents. The centroid of the peaks is pinned at 2.32 keV with an M value $\sim 71\%$.

Please note that typical values for M , according to other studies using thermionic e-impact energy $E_e = 150 \text{ keV}$ on W anode, are the range of 15%–18% after filtration.⁷ The values obtained for FWHM are in the range of 6–10 keV for operating E_e from 30 to 70 keV, coupled with a sharp decrease of the signal intensity resulting from the presence of the filters.⁵

2. L-peak intensity vs. field emission current

Equation (2) specifies that the intensity of the L-peak is also e-beam current dependant. An increase in the FE current for the same FE voltage can be achieved by using the array of independently powered FE tips, with mostly the same FE characteristics, as used in this study with the 7-CNP-tip array. This is done by activating more or less the number of CNP tips of the cathode array at the same FE voltage. In order to quantify the relationship between the peak intensity and the e-impact current, we have measured the x-ray energy spectra for same e-impact energy E_e but with different FE currents. An example of the spectrum variation is presented in Fig. 8. This figure shows a conservation of the L-peak characteristics, i.e., same centroid and FWHM, as well as a preservation of the M value. Moreover, there is an almost linear increase of the peak intensity with the FE current. This means experimentally that the intensity of the x-ray emission can be easily modified by the FE current, without losing its monochromatic specificity. This possibility to increase the

TABLE I. Outermost L-shell emission lines²⁶ and assumed centroid of the merged L-peak with minimum values for the FWHM for different counter-anode materials. λ is the wavelength corresponding to the L-peak.

	Ti	Co	Cu	Ge	Mo	Pd	Ag
$L_{\alpha 1}$ (keV)	0.45	0.78	0.93	1.19	2.29	2.84	2.98
L_{β}/L_{γ} (keV)	0.46	0.79	0.95	1.22	2.62	3.33	3.52
L-peak (keV)	0.46	0.79	0.94	1.21	2.46	3.09	3.25
FWHM (keV)	0.01	0.01	0.02	0.03	0.33	0.49	0.54
λ (nm)	2.72	1.58	1.32	1.03	0.50	0.40	0.38

TABLE II. L-shell emission lines²⁶ and the assumed centroids corresponding to two distinct L_{α} -peak and L_{β} -peak, for different counter-anode materials. λ is the wavelength corresponding to the L-peak.

	Ta	W	Re	Ir	Pt	Au
$L_{\alpha 1}$ (keV)	8.15	8.40	8.65	9.17	9.44	9.71
$L_{\alpha 2}$ (keV)	8.09	8.34	8.59	9.10	9.36	9.63
L_{α} - peak (keV)	8.12	8.37	8.62	9.13	9.40	9.67
FWHM (keV)	0.06	0.06	0.06	0.07	0.08	0.08
λ (nm)	0.15	0.15	0.14	0.14	0.13	0.13
$L_{\beta 1}$ (keV)	9.34	9.67	10.01	10.71	11.07	11.44
$L_{\beta 2}$ (keV)	9.65	9.96	10.28	10.92	11.25	11.58
L_{β} - peak (keV)	9.50	9.82	10.14	10.81	11.16	11.51
FWHM (keV)	0.31	0.29	0.27	0.21	0.18	0.14
λ (nm)	0.13	0.13	0.12	0.11	0.11	0.11

impact FE current for a given E_e will counterbalance the low yield of soft x-ray emission.

C. Changing the x-ray wavelength

The wavelength of the x-ray source can be modified by the choice of target material. Two cases can be considered depending on the target material:

- (1) All the L-shell emission lines are within an energy range of less than ~ 500 eV. In such case we assume that all emission lines will merge to form a single L-peak, as indicated by our experimental results with Mo. As the first estimate, the centroid of the L-peak is located roughly at the center of the energy interval between the emission lines, and its FWHM should have a lower limit defined by the emission line energy interval. As detailed in Table I, for instance, we have calculated the position of these L-peaks for different materials presenting such specificity and we have also provided the wavelengths λ associated with the L-peak energies. The main properties of these x-ray sources should be similar to those presented for Mo in this article. Deviations between experiment and theoretical prediction depend mostly on the transition cross-sections that give rise to the emission lines.
- (2) The distribution of the L-shell emission lines presents dispersion in energy that is too important to lead to a merger into one single L-peak. This is the case of materials presented in Table II, for example. Under such a condition, the x-ray spectrum consists of two distinct L-peaks, an L_{α} -peak and a L_{β} -peak. However, the L-peak intensities being a function of U_L (Eqs. (3) and (4)), the first L_{α} -peak intensity should prevail over the L_{β} -peak, because E_e is closer to the L_{β} -peak. Therefore, the monochromaticity of the L_{α} -peaks will be more dependent on E_e than in case (1). Please also note in this case the small values of the FWHM of the L_{α} -peaks.

V. CONCLUSIONS

By favoring the L-peak emission over the bremsstrahlung part, direct quasi-monochromatic soft x-ray emission is obtained. This has been enabled by the high brightness of

the FE e-beam coupled with an array structure of the cold cathode which allows an easy control of the x-ray emission intensity.

Future development of such quasi-monochromatic FE x-ray sources should also take advantage of two other FE e-beam characteristics – easy e-beam focus, for developing x-ray point source,²⁷ and high frequency switching⁴ in a simple configuration – which allow compact x-ray systems to be in the range of sub-millimeter. This suggests potential applications for the presented quasi-monochromatic soft FE x-ray for high resolution phase contrast imaging,^{28–31} either in microradiology or microtomography. Finally, new developments in coherent soft x-ray radiotherapy and nanolithography could be considered by the use, either individually or in concomitance, of the following specificities related to the quasi-monochromatic FE x-ray sources: ambient working temperature, directional and high brightness e-beam, high x-ray yield, extreme miniaturization made possible by the simple configuration, and direct monochromaticity.

¹V. T. Binh, in *The Oxford Handbook of Nanoscience and Technology: Volume III: Applications*, edited by A. V. Narlikar and Y. Y. Fu (Oxford University Press, New York, 2010), pp. 736–788.

²S. Wang, O. Zhou and S. Chang, in *The Oxford Handbook of Nanoscience and Technology: Volume III: Applications*, edited by A. V. Narlikar and Y. Y. Fu (Oxford University Press, New York, 2010), pp. 673–698.

³S. Senda, Y. Sakai, Y. Mizuta, S. Kita, and F. Okuyama, *Appl. Phys. Lett.* **85**(23), 5679–5681 (2004).

⁴G. Yue, Q. Qiu, B. Gao, Y. Cheng, J. Zhang, H. Shimoda, S. Chang, J. Lu, and O. Zhou, *Appl. Phys. Lett.* **81**(2), 355–357 (2002).

⁵R. T. Lopes, E. B. Costab, and E. F. O. de Jesus, *Appl. Radiat. Isot.* **53**, 665–671 (2000).

⁶G. G. Poludniowski, *Med. Phys.* **34**(6), 2175–2186 (2007).

⁷G. Harding, B. David, A. Harding, A. Thran, and J. P. Schlomka, *Radiat. Phys. Chem.* **76**(7), 1116–1121 (2007).

⁸A. Levesque, V. T. Binh, V. Semet, D. Guillot, R. Y. Fillit, M. D. Brookes, and T. P. Nguyen, *Thin Solid Films* **464**, 308–314 (2004).

⁹H. A. Kramers, *Philos. Mag.* **46**(275), 836–871 (1923).

¹⁰D. M. Tucker, G. T. Barnes, and D. P. Chakraborty, *Med. Phys.* **18**(2), 211–218 (1991).

¹¹K. Shima, M. Okuda, E. Suzuki, T. Tsubota, and T. Mikumo, *J. Appl. Phys.* **54**(3), 1202–1208 (1983).

¹²A. Vignes and G. Dez, *J. Phys. D* **1**(10), 1309–1322 (1968).

¹³J. M. Boone, in *Handbook of Medical Imaging: Volume 1. Physics and Psychophysics*, edited by H. L. K. J. Beutel and R. L. Van Metter (SPIE-The International Society for Optical Engineering, Bellingham, WA, 2000), pp. 3–78.

¹⁴E. Sato, E. Tanaka, H. Mori, T. Kawai, T. Ichimaru, S. Sato, K. Takayama, and H. Ido, *Med. Phys.* **32**(1), 49–54 (2005).

¹⁵Amptek X123 ($3 \times 3 \times 1$ mm³ detector/100 μ m Be window/EXV5 5 inch detector extension); R. H. Redus, A. Huber, J. Pantazis, T. Pantazis, and D. Sperry, *IEEE Nucl. Sci. Symp. Conf. Rec. R15-4* (2006).

¹⁶Q. H. Wang, T. D. Corrigan, J. Y. Dai, R. P. H. Chang, and A. R. Krauss, *Appl. Phys. Lett.* **70**(24), 3308–3310 (1997).

¹⁷V. Semet, V. T. Binh, P. Vincent, D. Guillot, K. B. K. Teo, M. Chhowalla, G. A. J. Amarantunga, W. I. Milne, P. Legagneux, and D. Pribat, *Appl. Phys. Lett.* **81**(2), 343–345 (2002).

¹⁸M. Mauger and V. T. Binh, *J. Vac. Sci. Technol. B* **24**(2), 997–1003 (2006).

¹⁹M. Mauger, R. Mouton, O. Hamzaoui, and V. T. Binh, *J. Vac. Sci. Technol. B* **25**(2), 575–578 (2007).

²⁰A. Levesque, P. Vincent, V. T. Binh, D. Guillot, and M. D. Brookes, *J. Vac. Sci. Technol. B* **23**(2), 665–670 (2005).

²¹R. Mouton, V. Semet, D. Guillot, and V. T. Binh, *J. Vac. Sci. Technol. B* **24**(2), 993–996 (2006).

²²V. T. Binh, M. Brookes, V. Semet, R. Mouton, D. Kilgour, and I. Jupp, paper presented at the Gordon Research Conferences on Detecting Illicit Substances: Explosives & Drugs, Big Sky, Montana, 16–21 September 2007 (unpublished).

- ²³R. Mouton, V. Semet, D. Kilgour, M. D. Brookes, and V. T. Binh, *J. Vac. Sci. Technol. B* **26**(2), 755–759 (2008).
- ²⁴C. Oshima, K. Mastuda, T. Kona, Y. Mogami, M. Komaki, Y. Murata, T. Yamashita, T. Kuzumaki, and Y. Horiike, *Phys. Rev. Lett.* **88**(3), 038301 (2002).
- ²⁵A. Mayer, N. M. Miskovsky, and P. H. Cutler, *Phys. Rev. B* **65**(15), 155420 (2002).
- ²⁶J. B. Kortright and A. C. Thompson, *CXRO X-Ray Data Booklet* (Lawrence Berkeley National Laboratory, University of California, 2009).
- ²⁷W. Sugimoto, S. Sugita, Y. Sakai, H. Goto, Y. Watanabe, Y. Ohga, S. Kita, and T. Ohara, *J. Appl. Phys.* **108**(4), 044507 (2010).
- ²⁸Y. Hwu, W.-L. Tsai, A. Groso, G. Margaritondo, and J. H. Je, *J. Phys. D* **35**, R105–R120 (2002).
- ²⁹A. Momose, *Jpn. J. Appl. Phys.* **44**(9A), 6355–6367 (2005).
- ³⁰B. M. Weon, J. H. Je, Y. Hwu, and G. Margaritondo, *Int. J. Nanotechnol.* **3**(2/3), 280–297 (2006).
- ³¹B. Zoofan, J.-Y. Kim, and S. I. Rokhlin, *J. Appl. Phys.* **100**, 014502 (2006).